MATERIALS CHEMISTRY
FRONTIERS

CHINESE CHEMICAL SOCIETY

ROYAL SOCIETY OF CHEMISTRY

RESEARCH ARTICLE

View Article Online
View Journal | View Issue

Check for updates

Cite this: *Mater. Chem. Front.*, 2020, 4, 1643

Near-IR absorption and photocurrent generation using a first-of-its-kind boron difluoride formazanate non-fullerene acceptor†

Josh D. B. Koenig,[a] Mahmoud E. Farahat,[a] Jasveer S. Dhindsa,[b] Joe B. Gilroy *[b] and Gregory C. Welch *[a]

Received 26th February 2020,
Accepted 6th April 2020

DOI: 10.1039/d0qm00109k

rsc.li/frontiers-materials

Herein, we report the synthesis and characterization of the first non-fullerene acceptor (NFA) containing a boron difluoride formazanate (**BF_2fz**) core end-capped with N-annulated perylene diimides (PDIs). Electronic coupling between the **BF_2fz** core and the PDI endcaps enabled tuning of the lowest unoccupied molecular orbital, leading to near-panchromatic optical absorption. Post-deposition solvent vapor annealing of the new NFA resulted in a significant red-shift in the optical spectra, which stretched into the near-IR. Proof-of-concept organic photovoltaic (OPV) devices were constructed to demonstrate the potential of this new material as an NFA. SVA treatment of the active layer resulted in a 2-fold increase in power conversion efficiency (PCE), due mainly to increases in the **BF_2PDI_2** generated photocurrent that extended into the near-IR.

Introduction

For applications in organic photovoltaics (OPVs), π-conjugated materials are perfectly suited for use as non-fullerene acceptors (NFAs) because both physical and optoelectronic properties may be optimized to match the electron-donor material with which they are paired in the active layer.[1,2] One class of non-fullerene acceptors (NFAs) recognized for high redox and thermal stability, as well as high molar absorptivity, are perylene diimides (PDIs).[3,4] Despite such favorable qualities, the efficiency of charge-extraction for PDI-based NFA materials is often hindered by the formation of large π–π stacking domains throughout the BHJ.[1] To promote more favorable phase separation in the BHJ, PDI self-assembly may be disrupted through either direct dimerization of PDIs[5–8] or insertion of a core between the PDI-moieties.[9–20]

The Welch research group has previously explored the opto-electronic influence of thienoisoindigo, thienyl- and pyridyl-diketopyrrolopyrrole cores that were acetylene-linked to N-annulated PDI (Fig. 1).[21] Strong electronic communication between the cores and PDI endcaps adjusted the highest occupied molecular orbital (HOMO) energy level of these molecules, affording near-panchromatic absorptions ideally suited for OPV. In search of a core that could achieve similar absorptivity, while instead influencing the lowest unoccupied molecular (LUMO) energy level, we targeted an acetylene-terminated boron difluoride formazanate (**BF_2fz**), a chromophore popularized by the Gilroy research group.[22–24] The properties of **BF_2fz** materials are highly sensitive to structural variation at the *N*-aryl substituents,[25–27] meaning the optoelectronic properties can be tuned by the choice of endcap material. In this contribution, we report the synthesis, characterization, and NFA capability of a new π-conjugated material comprised of a **BF_2fz** core acetylene-linked to N-annulated PDI endcaps (**BF_2PDI_2**).

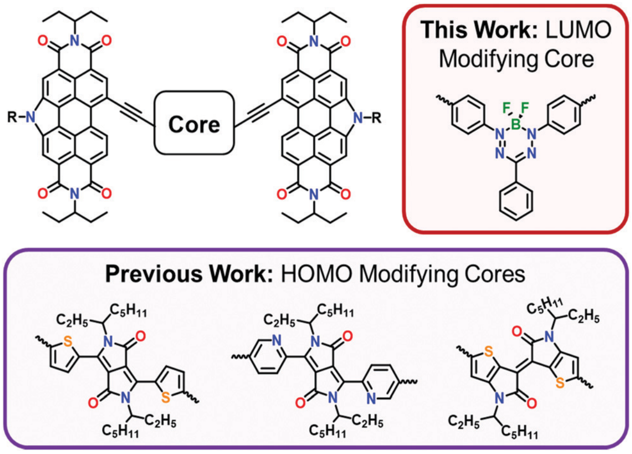

Fig. 1 Depicting previously investigated HOMO-modifying and newly synthesized LUMO-modifying N-annulated PDI-core-PDI materials. R = hexyl (HOMO modifying cores) or 2-ethylhexyl (LUMO modifying core).

---

[a] *Department of Chemistry, University of Calgary, Calgary, Alberta, T2N 1N4, Canada. E-mail: gregory.welch@ucalgary.ca; Tel: +1-403-210-7603*

[b] *Department of Chemistry and the Centre for Advanced Materials and Biomaterials Research (CAMBR), The University of Western Ontario, London, ON, N6A 5B7, Canada. E-mail: joe.gilroy@uwo.ca; Tel: +1-519-661-2111 ext. 81561*

† Electronic supplementary information (ESI) available. See DOI: 10.1039/d0qm00109k

Characterization

The **BF_2fz** core[22] and N-annulated PDI (Br-PDIN-EH)[8] end caps were connected *via* a Sonogashira cross-coupling reaction to generate **BF_2PDI_2** (see ESI,† for full experimental details). The identity of **BF_2PDI_2** was confirmed by ^1H, ^{11}B, ^{13}C, and ^{19}F NMR spectroscopy, as well as MALDI TOF mass spectrometry and CHN elemental analysis (Fig. S1–S7, ESI†). The ^{11}B and ^{19}F NMR spectra exhibited diagnostic 1 : 2 : 1 triplet and 1 : 1 : 1 : 1 quartet coupling patterns, respectively.[25] Moreover, the ^1H NMR spectrum showed no evidence of a formazan related N-H peak (at ~15 ppm),[22] strongly suggesting the **BF_2fz** core remained intact throughout synthesis and purification.

The thermal properties of **BF_2PDI_2** were measured using a combination of differential scanning calorimetry and thermal gravimetric analysis (Fig. S8 and S9, ESI†). No obvious glass transitions or melting points were observed between 100–300 °C, while the onset of molecular decomposition was not observed until > 300 °C. The high thermal stability observed in **BF_2PDI_2** may be attributed to significant π-conjugation between the **BF_2fz** core and the N-annulated PDI endcaps. This notion was supported by the density functional theory (DFT) optimized structure of **BF_2PDI_2** at the B3LYP-6-31G(d,p) level of theory (Fig. S14, ESI†). The PDI units were nearly co-planar with each other, with only a small degree of bending caused by the **BF_2fz** core. This DFT optimized 'dragonfly' structure corresponded well with previously determined X-ray crystallography structures for compounds using the same **BF_2fz** core.[23,24]

Next, the electronic properties of **BF_2PDI_2** were probed using cyclic voltammetry (CV), with additional information provided by DFT calculations. The CV of **BF_2PDI_2** was comprised of three irreversible oxidation events, as well as four fully reversible reduction events (Fig. 2). While the number oxidation events could be determined by differential pulse voltammetry (Fig. S13, ESI†), the precise electrochemical origin may not be readily assigned. On the other hand, the first and fourth reductions ($E_{1/2}$ = −0.85 and −1.96 V *vs.* $Fc^{+/0}$) may be attributed to **BF_2fz** core, while the second and third reduction events ($E_{1/2}$ = −1.32 and −1.60 V *vs.* $Fc^{+/0}$) may be attributed to N-annulated PDI as the current passed during these redox processes was 2× larger. By DFT calculations, the first oxidation event appeared to be delocalized across the entire molecule, while the first reduction event was largely centered on the **BF_2fz** core (Fig. S15, ESI†). The predicted HOMO–LUMO energy levels correlate well with the observed CV data. Together, these data strongly suggest that the **BF_2fz** core has a higher electron affinity than the N-annulated PDI endcaps, which served to lower the LUMO energy level of **BF_2PDI_2**, when compared to related compounds with different cores.[21]

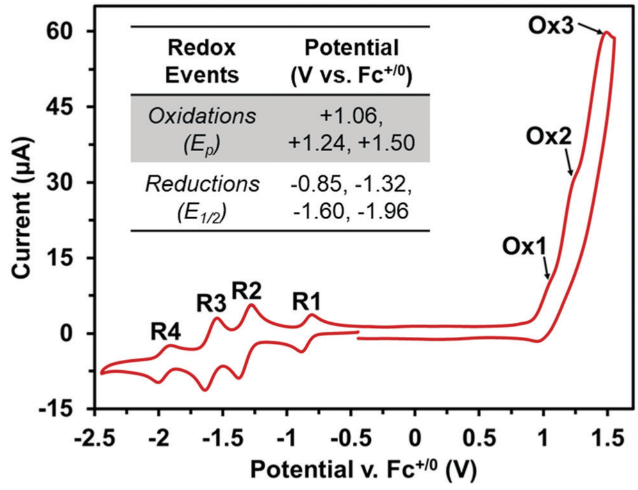

Redox Events	Potential (V vs. $Fc^{+/0}$)
Oxidations (E_p)	+1.06, +1.24, +1.50
Reductions ($E_{1/2}$)	-0.85, -1.32, -1.60, -1.96

Fig. 2 Cyclic voltammogram of **BF_2PDI_2**, measured at 100 mV s^{-1} in CH_2Cl_2 under argon with 0.1 M $TBAPF_6$ supporting electrolyte (WE = glassy carbon, CE = Pt-wire, *pseudo*-RE = Ag/AgCl). Inset are all measured oxidation (Ox) and reduction (R) events, referenced to $Fc^{+/0}$.

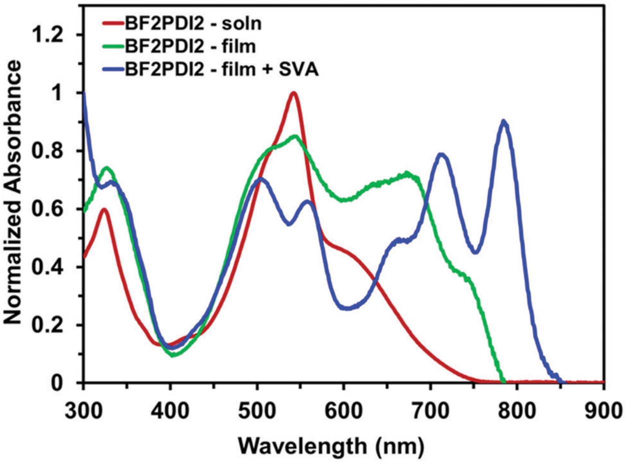

Fig. 3 UV-vis-nIR absorption profile of **BF_2PDI_2** in $CHCl_3$ solution (red), thin-film spin-cast from *o*-dichlorobenzene (green), and the same thin-film solvent vapor annealed from $CHCl_3$ (blue).

The optical properties of **BF_2PDI_2** were measured by UV-visible-nearIR absorption spectroscopy (UV-vis-nIR). The UV-vis-nIR profile of **BF_2PDI_2** in solution exhibited a broad absorbance between 450–750 nm, with an absorption maximum (λ_{max}) at 543 nm attributable to the PDI endcaps and a low energy shoulder just beyond 600 nm attributed to the **BF_2fz** core (Fig. 3). By overlaying the optical spectra of **BF_2PDI_2** with its constituent fragments (BF_2Ace_2 and PDIN-EH, Fig. S11, ESI†), it was revealed that the low energy shoulder attributed to **BF_2fz** core was red-shifted in **BF_2PDI_2**, emphasizing the extension of π-conjugation induced by the PDI endcaps. When spin-cast into a thin-film, the optical profile of **BF_2PDI_2** underwent several notable changes. Beyond the slightly red-shifted onset of absorption (λ_{onset}), the broadening of λ_{max} was also accompanied by an appreciable increase in the intensity of the low-energy shoulder, consistent with enhanced electron delocalization along the π-conjugated backbone.[21]

In the past, we have shown that post-deposition solvent vapor annealing (SVA) can induce structural order within the solid-state morphology of similar PDI–core–PDI materials.[11,28–31] Exposure of the **BF_2PDI_2** thin-film to $CHCl_3$ solvent vapors caused the once broad solid-state optical profile to resolve into two distinct absorption regions. The PDI-based λ_{max} region was split into two peaks (λ = 508 and 560 nm), while the low-energy shoulder

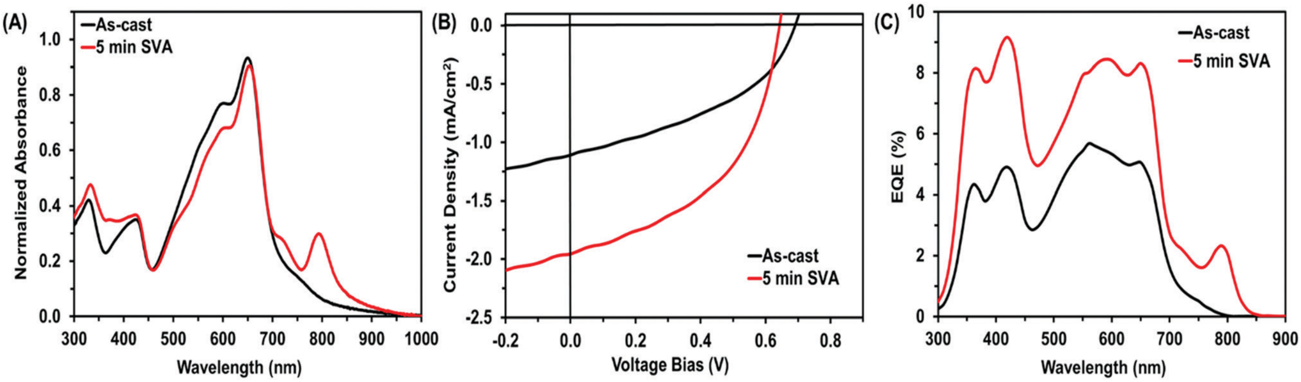

Fig. 4 Optical absorption profile (A), *J*–*V* curves (B), an external quantum efficiency plots (C) comparing the effects of solvent vapor annealing with $CHCl_3$ on ternary blend OPV devices with a FBT : $\mathbf{BF_2PDI_2}$: $PC_{61}BM$ (1 : 1 : 0.5) active layer at 10 mg mL^{-1} total concentration.

developed fine structure (λ_{max} = 790 nm) that extended well into the near-IR (λ_{onset} = 850 nm). This behaviour is strongly indicative of molecular reorganization and/or aggregation of $\mathbf{BF_2PDI_2}$ into ordered domains with strong intermolecular electronic-coupling in the solid-state.[32–34]

OPV devices

The NFA capabilities of $\mathbf{BF_2PDI_2}$ were assessed by constructing some proof-of-concept OPV devices with the following inverted architecture: ITO/ZnO/ternary active layer/MoOx/Ag (full experimental details in ESI†). A ternary active layer comprised of electron-donor polymer PPDT2FBT (FBT), $PC_{61}BM$, and $\mathbf{BF_2PDI_2}$ was employed for OPV devices. FBT was selected because of its complementary absorption with the solvent vapor annealed film of $\mathbf{BF_2PDI_2}$ (Fig. S16, ESI†). $PC_{61}BM$ was added to this ternary blend to assist with charge mobility.[35] Using a FBT : $\mathbf{BF_2PDI_2}$: $PC_{61}BM$ blend ratio of (1 : 1 : 0.5) at 10 mg mL^{-1} total concentration, the best OPV devices achieved an open circuit voltage (V_{oc}) of 0.69 V, a short circuit current (J_{sc}) of 1.1 mA cm^{-2}, and a fill factor (FF) of 41%, leading to a power conversion efficiency (PCE) of 0.3% (Table S1, ESI†).

Post-deposition treatment of these films with $CHCl_3$ SVA resulted in the desired optical profile shift of $\mathbf{BF_2PDI_2}$, giving the OPV devices a near-panchromatic absorbance (Fig. 4A). Device performance was maximized after 5 min of $CHCl_3$ SVA, where both the J_{sc} and FF increased to 1.9 mA cm^{-2} and 49%, respectively, leading to a 2-fold increase in PCE to 0.6% (Fig. 4B). Longer SVA treatments led to OPV performances similar to as-cast devices (Fig. S17 and Table S2, ESI†). This phenomena has previously been observed with our N-annulated PDI–core–PDI materials and was attributed to over-annealing of the active layer.[11,28]

To better understand the observed enhancement in OPV performance for FBT : $\mathbf{BF_2PDI_2}$: $PC_{61}BM$ (1 : 1 : 0.5) ternary blends that were SVA using $CHCl_3$ for 5 min, photoluminescence (PL) and external quantum efficiency (EQE) experiments were performed. PL measurements of the ternary blend showed efficient quenching of the FBT polymer before and after SVA treatment (Fig. S18, ESI†). Analysis of the EQE spectra, the measured photocurrent clearly displays contributions from all components of the ternary blend (Fig. 4C). Following SVA treatment, photocurrent generation was extended well into the near-IR (λ_{max} = 790 nm), clearly emphasizing the increased contribution from the new NFA material, $\mathbf{BF_2PDI_2}$.

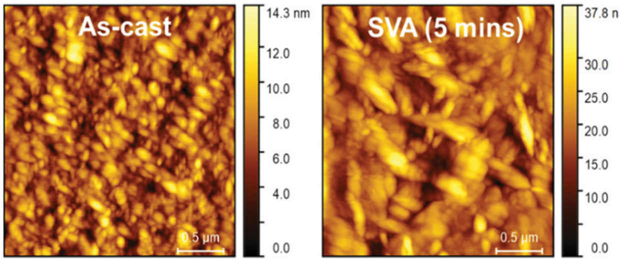

Fig. 5 Atomic force microscopy height images of ternary blend OPV devices with an FBT : $\mathbf{BF_2PDI_2}$: $PC_{61}BM$ (1 : 1 : 0.5) active layer at 10 mg mL^{-1} total concentration.

Surface morphology differences between the as-cast and SVA treated devices were also analyzed by atomic force microscopy (AFM). AFM height images showed significant differences between the as-cast and SVA treated devices (Fig. 5), as the root-mean square surface roughness of the films increased from 1.9 nm to 4.8 nm. X-ray diffraction (XRD) measurements of ternary blend films before and after $CHCl_3$ SVA failed to show any distinguishing features that could be attributed to $\mathbf{BF_2PDI_2}$ (Fig. S19, ESI†).[36] Together, these data suggest that SVA enhanced OPV performance by inducing $\mathbf{BF_2PDI_2}$ aggregation into phase separated domains, rather than crystallization.

Conclusions

In conclusion, we have synthesized and fully characterized a first-of-its-kind NFA containing a $\mathbf{BF_2fz}$ core. The use of acetylene-linkers enabled through-conjugation between the $\mathbf{BF_2fz}$ core and the PDI endcaps, leading to an altered LUMO energy level that resulted in near-panchromatic absorption for $\mathbf{BF_2PDI_2}$. The new compound is a rare example of an acceptor–acceptor–acceptor type π-conjugated architecture. Treatment of solid-state $\mathbf{BF_2PDI_2}$ with $CHCl_3$ SVA resulted in a significant bathochromic shift of the optical spectra, leading to near-IR absorption. The overall performance in a series of proof-of-concept OPV devices, where **BF_2PDI_2** was used as an NFA in a ternary blend system, was improved 2-fold by SVA treatment of the active layer. The increase in PCE could be mainly attributed to favorable aggregation of **BF_2PDI_2** in the active layer which increased the generated photocurrent. This notion was supported by EQE and AFM measurements. This work demonstrates the utility of the **BF_2fz** organic dye to construct narrow bandgap π-conjugated materials for use in organic electronics and provides the groundwork for further development.

Conflicts of interest

There are no conflicts to declare.

Acknowledgements

GCW acknowledges the Canada Research Chairs Program, CFI JELF (34102), NSERC DG (2019-04392), and the University of Calgary. JBG acknowledges CFI JELF (33977), NSERC DG (2018-04240), and the University of Western Ontario. JSD acknowledges NSERC CGS-D Scholarship. JK acknowledges Alberta Graduate Excellence Scholarship (AGES) program. Compute Canada and Westgrid are acknowledged for computational resources. This research was undertaken thanks in part to funding from the Canada First Research Excellence Fund (CFREF).

References

1 S. Rajaram, R. Shivanna, S. K. Kandappa and K. S. Narayan, Nonplanar Perylene Diimides as Potential Alternatives to Fullerenes in Organic Solar Cells, *J. Phys. Chem. Lett.*, 2012, **3**, 2405–2408.

2 C. B. Nielsen, S. Holliday, H.-Y. Chen, S. J. Cryer and I. McCulloch, Non-Fullerene Electron Acceptors for Use in Organic Solar Cells, *Acc. Chem. Res.*, 2015, **48**, 2803–2812.

3 Z. Liu, Y. Wu, Q. Zhang and X. Gao, Non-Fullerene Small Molecule Acceptors Based on Perylene Diimides, *J. Mater. Chem. A*, 2016, **4**, 17604–17622.

4 W. Chen and Q. Zhang, Recent Progress in Non-Fullerene Small Molecule Acceptors in Organic Solar Cells (OSCs), *J. Mater. Chem. C*, 2017, **5**, 1275–1302.

5 D. Sun, D. Meng, Y. Cai, B. Fan, Y. Li, W. Jiang, L. Huo, Y. Sun and Z. Wang, Non-Fullerene-Acceptor-Based Bulk-Heterojunction Organic Solar Cells with Efficiency over 7%, *J. Am. Chem. Soc.*, 2015, **137**, 11156–11162.

6 D. Meng, D. Sun, C. Zhong, T. Liu, B. Fan, L. Huo, Y. Li, W. Jiang, H. Choi, T. Kim, J. Y. Kim, Y. Sun, Z. Wang and A. J. Heeger, High-Performance Solution-Processed Non-Fullerene Organic Solar Cells Based on Selenophene-Containing Perylene Bisimide Acceptor, *J. Am. Chem. Soc.*, 2016, **138**, 375–380.

7 A. D. Hendsbee, J.-P. Sun, W. K. Law, H. Yan, I. G. Hill, D. M. Spasyuk and G. C. Welch, Synthesis, Self-Assembly, and Solar Cell Performance of N-Annulated Perylene Diimide Non-Fullerene Acceptors, *Chem. Mater.*, 2016, **28**, 7098–7109.

8 S. V. Dayneko, A. D. Hendsbee and G. C. Welch, Combining Facile Synthetic Methods with Greener Processing for Efficient Polymer-Perylene Diimide Based Organic Solar CellsSmall, *Methods*, 2018, **2**, 1800081.

9 Y. Lin, Y. Wang, J. Wang, J. Hou, Y. Li, D. Zhu and X. Zhan, A Star-Shaped Perylene Diimide Electron Acceptor for High-Performance Organic Solar Cells, *Adv. Mater.*, 2014, **26**, 5137–5142.

10 Y. Duan, X. Xu, H. Yan, W. Wu, Z. Li and Q. Peng, Pronounced Effects of a Triazine Core on Photovoltaic Performance–Efficient Organic Solar Cells Enabled by a PDI Trimer-Based Small Molecular Acceptor, *Adv. Mater.*, 2017, **29**, 1605115.

11 S. M. McAfee, S. V. Dayneko, P. Josse, P. Blanchard, C. Cabanetos and G. C. Welch, Simply Complex: The Efficient Synthesis of an Intricate Molecular Acceptor for High-Performance Air-Processed and Air-Tested Fullerene-Free Organic Solar Cells, *Chem. Mater.*, 2017, **29**, 1309–1314.

12 J. Liu, S. Xie, S. Feng, M. Li, L. Wu, X. Xu, X. Chen, C. Li and Z. Bo, A Propeller-Shaped Perylene Diimide Hexamer as a Nonfullerene Acceptor for Organic Solar Cells, *J. Mater. Chem. C*, 2018, **6**, 9336–9340.

13 H. Lin, S. Chen, H. Hu, L. Zhang, T. Ma, J. Y. L. Lai, Z. Li, A. Qin, X. Huang, B. Tang and H. Yan, Reduced Intramolecular Twisting Improves the Performance of 3D Molecular Acceptors in Non-Fullerene Organic Solar Cells, *Adv. Mater.*, 2016, **28**, 8546–8551.

14 Q. Wu, D. Zhao, A. M. Schneider, W. Chen and L. Yu, Covalently Bound Clusters of Alpha-Substituted PDI—Rival Electron Acceptors to Fullerene for Organic Solar Cells, *J. Am. Chem. Soc.*, 2016, **138**, 7248–7251.

15 J. Zhang, Y. Li, J. Huang, H. Hu, G. Zhang, T. Ma, P. C. Y. Chow, H. Ade, D. Pan and H. Yan, Ring-Fusion of Perylene Diimide Acceptor Enabling Efficient Nonfullerene Organic Solar Cells with a Small Voltage Loss, *J. Am. Chem. Soc.*, 2017, **139**, 16092–16095.

16 Q. Zhang, X. Xu, S. Chen, G. B. Bodedla, M. Sun, Q. Hu, Q. Peng, B. Huang, H. Ke, F. Liu, T. P. Russell and X. Zhu, Phenylene-Bridged Perylenediimide-Porphyrin Acceptors for Non-Fullerene Organic Solar Cells, Sustain, *Energy Fuels*, 2018, **2**, 2616–2624.

17 T. A. Welsh, A. Laventure, T. Baumgartner and G. C. Welch, Dithienophosphole-Based Molecular Electron Acceptors Constructed Using Direct (Hetero)Arylation Cross-Coupling Methods, *J. Mater. Chem. C*, 2018, **6**, 2148–2154.

18 T. A. Welsh, A. Laventure, A. F. Alahmadi, G. Zhang, T. Baumgartner, Y. Zou, F. Jäkle and G. C. Welch, Borane Incorporation in a Non-Fullerene Acceptor To Tune Steric and Electronic Properties and Improve Organic Solar Cell Performance, *ACS Appl. Energy Mater.*, 2019, **2**, 1229–1240.

19 Z. Luo, T. Liu, Z. Chen, Y. Xiao, G. Zhang, L. Huo, C. Zhong, X. Lu, H. Yan, Y. Sun and C. Yang, Isomerization of Perylene Diimide Based Acceptors Enabling High-Performance Non-fullerene Organic Solar Cells with Excellent Fill Factor, *Adv. Sci.*, 2019, **6**, 1802065.

20 J. D. B. Koenig, A. Laventure and G. C. Welch, Harnessing Direct (Hetero)Arylation in Pursuit of a Saddle-Shaped Perylene Diimide Tetramer, *ACS Appl. Energy Mater.*, 2019, **2**, 8939–8945.

21 J. R. Cann, C. Cabanetos and G. C. Welch, Spectroscopic Engineering toward Near-Infrared Absorption of Materials Containing Perylene Diimide, *ChemPlusChem*, 2017, **82**, 1359–1364.

22 S. M. Barbon and J. B. Gilroy, Boron Difluoride Formazanate Copolymers with 9,9-Di-*n*-Hexylfluorene Prepared by Copper-Catalyzed Alkyne–Azide Cycloaddition Chemistry, *Polym. Chem.*, 2016, **7**, 3589–3598.

23 J. S. Dhindsa, R. R. Maar, S. M. Barbon, M. O. Avilés, Z. K. Powell, F. Lagugné-Labarthet and J. B. Gilroy, A π-Conjugated Inorganic Polymer Constructed from Boron Difluoride Formazanates and Platinum(II) Diynes, *Chem. Commun.*, 2018, **54**, 6899–6902.

24 J. S. Dhindsa, A. Melenbacher, S. M. Barbon, M. J. Stillman and J. B. Gilroy, Altering the Optoelectronic Properties of Boron Difluoride Formazanate Dyes *via* Conjugation with Platinum(II)-Acetylides, *Dalton Trans.*, 2020, DOI: 10.1039/C9DT03417J.

25 R. R. Maar, S. M. Barbon, N. Sharma, H. Groom, L. G. Luyt and J. B. Gilroy, Evaluation of Anisole-Substituted Boron Difluoride Formazanate Complexes for Fluorescence Cell Imaging, *Chem. – Eur. J.*, 2015, **21**, 15589–15599.

26 R. R. Maar, R. Zhang, D. G. Stephens, Z. Ding and J. B. Gilroy, Near-Infrared Photoluminescence and Electrochemiluminescence from a Remarkably Simple Boron Difluoride Formazanate Dye, *Angew. Chem., Int. Ed.*, 2019, **58**, 1052–1056.

27 J. B. Gilroy and E. Otten, Formazanate Coordination Compounds: Synthesis, Reactivity, and Applications, *Chem. Soc. Rev.*, 2020, **49**, 85–113.

28 S. M. McAfee, A.-J. Payne, S. V. Dayneko, G. P. Kini, C. E. Song, J.-C. Lee and G. C. Welch, A Non-Fullerene Acceptor with a Diagnostic Morphological Handle for Streamlined Screening of Donor Materials in Organic Solar Cells, *J. Mater. Chem. A*, 2017, **5**, 16907–16913.

29 S. M. McAfee, A.-J. Payne, A. D. Hendsbee, S. Xu, Y. Zou and G. C. Welch, Toward a Universally Compatible Non-Fullerene Acceptor: Multi-Gram Synthesis, Solvent Vapor Annealing Optimization, and BDT-Based Polymer Screening, *Sol. RRL*, 2018, **2**, 1800143.

30 D. Zomerman, J. Kong, S. M. McAfee, G. C. Welch and T. L. Kelly, Control and Characterization of Organic Solar Cell Morphology Through Variable-Pressure Solvent Vapor Annealing, *ACS Appl. Energy Mater.*, 2018, **1**, 5663–5674.

31 A.-J. Payne, N. A. Rice, S. M. McAfee, S. Li, P. Josse, C. Cabanetos, C. Risko, B. H. Lessard and G. C. Welch, Donor or Acceptor? How Selection of the Rylene Imide End Cap Impacts the Polarity of π-Conjugated Molecules for Organic Electronics, *ACS Appl. Energy Mater.*, 2018, **1**, 4906–4916.

32 A.-J. Payne, S. Li, S. V. Dayneko, C. Risko and G. C. Welch, An Unsymmetrical Non-Fullerene Acceptor: Synthesis via Direct Heteroarylation, Self-Assembly, and Utility as a Low Energy Absorber in Organic Photovoltaic Cells, *Chem. Commun.*, 2017, **53**, 10168–10171.

33 M. E. Farahat, C.-S. Tsao, Y.-C. Huang, S. Hsiung Chang, W. Budiawan, C.-G. Wu and C.-W. Chu, Toward Environmentally Compatible Molecular Solar Cells Processed from Halogen-Free Solvents, *J. Mater. Chem. A*, 2016, **4**, 7341–7351.

34 G. L. Schulz and S. Ludwigs, Controlled Crystallization of Conjugated Polymer Films from Solution and Solvent Vapor for Polymer Electronics, *Adv. Funct. Mater.*, 2017, **27**, 1603083.

35 S. B. Srivastava, S. K. Srivastava and S. P. Singh, Molecular-Shape-Induced Efficiency Enhancement in PC61BM and PC71BM Based Ternary Blend Organic Solar Cells, *J. Phys. Chem. C*, 2017, **121**, 17104–17111.

36 F. Tintori, A. Laventure and G. C. Welch, Additive Induced Crystallization of a Twisted Perylene Diimide Dimer within a Polymer Matrix, *Soft Matter*, 2019, **15**, 5138–5146.